Theoretical and Experimental Determination on Two Substrates Turned over by 4-Oxalocrotonate Tautomerase†

G. Andrés Cisneros,§,‡ Min Wang,§ Peter Silinski,§ Michael C. Fitzgerald,*,§ and Weitao Yang*,§

Department of Chemistry, Duke University, Box 90346, Durham, North Carolina 27708-0346, and Laboratory of Structural Biology, National Institute of Environmental Health Sciences, Research Triangle Park (RTP), North Carolina 27707

Received: August 4, 2005; In Final Form: September 9, 2005

Quantum mechanical/molecular mechanical (QM/MM) calculations and experimental kinetic studies have been performed on 4-oxalocrotonate tautomerase (4OT) for two different substrates, 2-hydroxymuconate (2HM) and 2-oxo-4-hexenedioate (2o4hex). Potential (ΔE) and free energy (ΔG) paths for both steps of the reaction using both substrates were calculated to determine the free energy barriers and compared to the experimental values obtained from the kinetic studies via the transition state theory. In the first step, a proton from the hydroxyl oxygen on the second carbon of 2HM, or from the third carbon of 2o4hex, is abstracted by Pro-1. In the second step, the proton is transferred to the fifth carbon of the substrate to form the product, 2-oxo-3-hexenedioate (2o3hex). For both substrates we obtain a calculated ΔG of $\approx$ 13 kcal/mol, in agreement with experimental determinations. The calculated free energy barrier difference $\Delta G_{2o4hex} - \Delta G_{2HM}$ ($\Delta\Delta G$) is 0.87 kcal/mol. We obtained an experimental $\Delta\Delta G$ of 0.85 kcal/mol. These results suggest that 2HM is turned over faster than 2o4hex by 4OT. However, these energy differences are so small that both 2HM and 2o4hex need to be taken into account in considering the mechanism of catalysis of 4OT.

I. Introduction

4-Oxalocrotonate tautomerase (4OT) is a homo-hexameric bacterial enzyme with 62 residues per subunit. It is part of a degradative metabolic pathway that converts various aromatic hydrocarbons to intermediates in the Krebs cycle. The plasmid that encodes 4OT has been determined to be the TOL plasmid pWW0.[1] This plasmid encodes the entire pathway and enables the bacteria to utilize various aromatic hydrocarbons as their sole sources of energy.[2] There are a total of six active sites in this protein, located in hydrophobic regions around the Pro-1 of each subunit. In particular, 4OT is responsible for the ketonization of 2-hydroxymuconate (2HM) and 2-oxo-4-hexenedioate (2o4hex) to its conjugated isomer 2-oxo-3-hexenedioate (see Figure 1).

Recent theoretical studies have shown that the reaction catalyzed by 4OT proceeds via a general acid−base mechanism without a general acid as shown in Figure 2.[3,4] In the first step, Pro-1 acts as the general base to abstract a proton from the hydroxyl oxygen on the second carbon of 2HM, or from the third carbon on 2o4hex. This results in the formation of a negative charge on the hydroxyl(carbonyl) oxygen that is stabilized by electrostatic interactions from Arg-39″ and an ordered water in the active site.[3] In the second step the proton is returned from Pro-1 to the fifth carbon of the product. The electrostatic stabilization role of Arg-39″ has been confirmed in recent experimental studies.[5]

This system presents an interesting case study since it is part of a cascade of reactions that enables *Pseudomonas putida mt-2*, a soil bacterium, to biodegrade aromatic compounds.

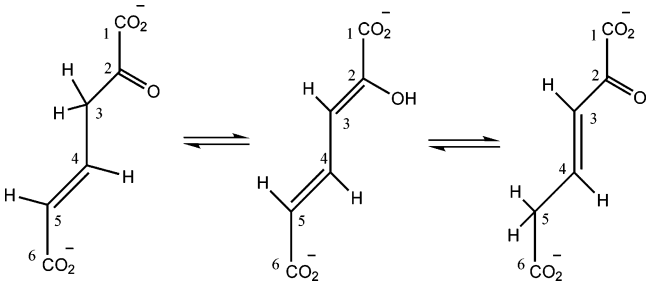

Figure 1. Isomerization reaction catalyzed by 4-OT.

Furthermore, several additional features make 4OT a particularly interesting system: it has a small monomer size (62 residues), 4OT catalyzes a proton-transfer reaction without the aid of any metal ion or cofactor, and the amino terminal Pro-1 acts as the general base, presenting a pK_a 3 units lower than that of the model compound. The reduction in the pK_a of proline has been explained by the fact that this residue is surrounded by hydrophobic residues, which produces a site with a low dielectric constant.[6,7]

Previous experiments to determine which substrate is turned over faster by 4OT have pointed to 2o4hex.[8] However, this is a difficult experiment since this substrate has never been isolated or synthesized. The determination of the kinetic parameters for 2o4hex have to be done indirectly. These parameters are obtained from an equilibrium experiment where 2HM is the substrate and a nonequilibrium experiment where both 2HM and 2o4hex are allowed to reach *kinetic* equilibrium. By using a velocity equation derived for a model in which two substrates compete for the same active site, the kinetic parameters for 2o4hex can be determined.[8]

In this contribution we have used a joint theoretical and experimental approach: a combined QM/MM method[9] devel-

† Part of the special issue "Donald G. Truhlar Festschrift".
§ Duke University.
‡ National Institute of Environmental Health Sciences.

10.1021/jp0543328 CCC: $33.50
Published on Web 10/14/2005

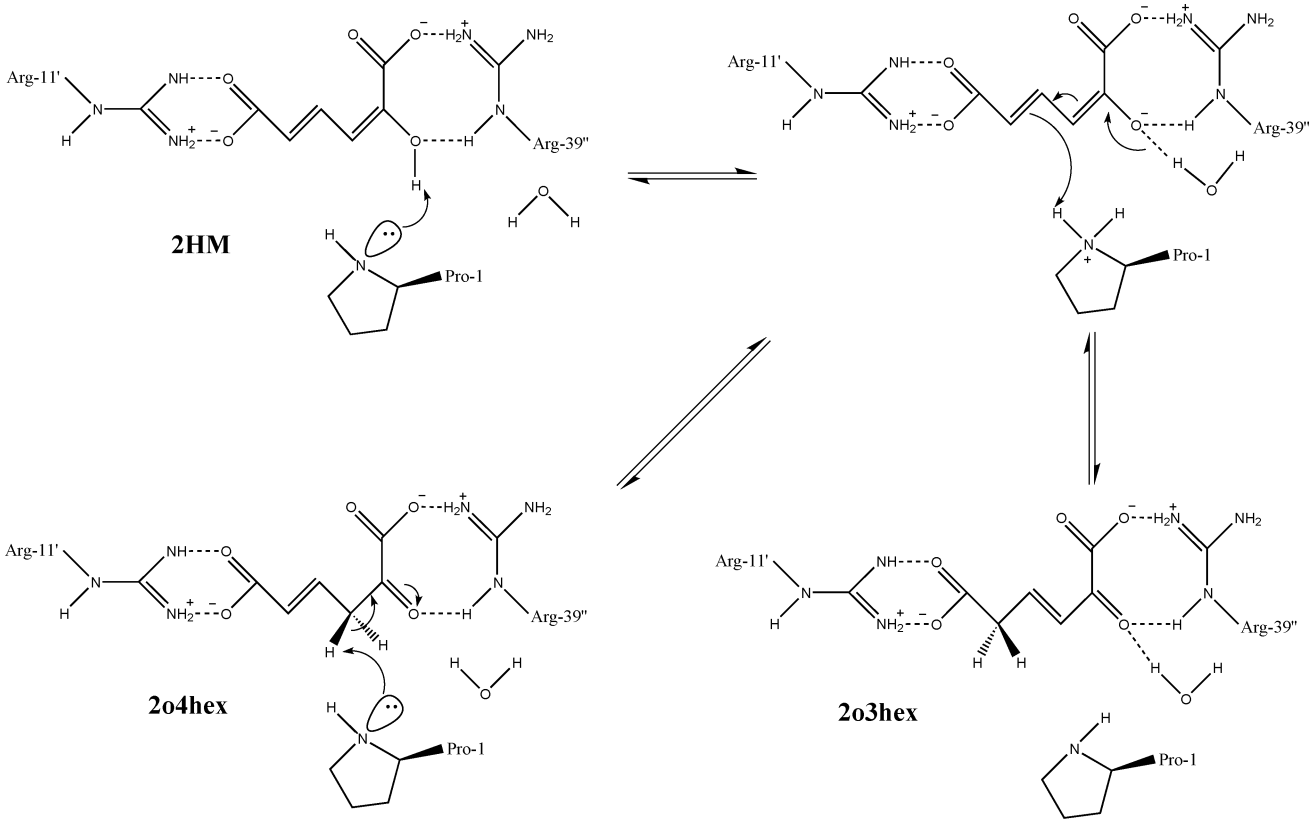

Figure 2. Proposed mechanism for 4-OT.[3,31]

oped recently in our laboratory,[10−14] and experimental determinations of kinetic parameters on 4OT to study both substrates in relation to each other, to obtain a better understanding of this enzyme's catalytic mechanism, and substrate turnover proficiency.

II. Methods

We now proceed to the description of the methods employed to determine the activation energies for both substrates. In subsection IIA we describe the computational methods as well as preparation of structures required for the QM/MM calculations. Subsequently, in subsection IIB the experimental methods are explained.

A. Computational Methods. *1. The QM/MM Potential Energy of Activation.* Our approach uses the pseudobond model of the QM/MM interface developed by Zhang et al.[10] All calculations were performed using QM/MM methodology[11,12] that has been implemented in a modified version of Gaussian 98,[15] which interfaces to a modified version of TINKER.[16] The AMBER95 all-atom force field parameter set[17] and the TIP3P model[18] for water were used.

A very important part of this QM/MM implementation is the use of the pseudobond model for the QM/MM boundary as developed in ref 10, which provides a smooth connection between the QM and the MM subsystems as well as an integrated expression for the potential energy of the overall system.

In the QM/MM potential energy model, the total energy of the system is

$$E_{\text{Total}} = E_{\text{MM}} + E_{\text{QM}} + E_{\text{QM/MM}} \qquad (1)$$

The QM/MM interactions ($E_{\text{QM/MM}}$) are taken to include bonded and nonbonded interactions. For the nonbonded interactions, the subsystems interact with each other through Lennard-Jones and point charge interaction potential. When the electronic structure is determined for the QM subsystem, the charges in the MM subsystem are included as a collection of fixed point charges in an effective Hamiltonian which describes the QM subsystem. That is, in the calculation of the QM subsystem we determine the contributions from the QM subsystem (E_{QM}), as well as the electrostatic contributions from the interaction between the QM and MM subsystems as explained by Zhang et al.[11]

The reaction paths are calculated by an iterative QM/MM procedure, developed by Cisneros et al.,[14] that combines two "chain of states" methods, the nudged-elastic-band (NEB) method[14,19,20] and the parallel path optimizer method.[13] In this procedure, the reaction paths are represented by a discrete set of structures which are optimized to the minimum energy path (MEP) in parallel. Initially only the reactant and product information are needed and the rest of the images are obtained by a linear interpolation between the end points. This parallel optimization is possible since any point on the MEP is a minimum in all directions except for the reaction coordinate. Thus, the energy gradient for any point is parallel to the local tangent of the reaction path.

In the QM/MM context, because of the large number of degrees of freedom, the system is partitioned into a core set and an environmental set.[13] For convenience the core set is defined by the atoms in the QM subsystem and the environment set is defined by the atoms in the MM subsystem. However, we note that these subsystems do not need to match. The systems are optimized iteratively with the core set being optimized first. At each point the subsystem not being optimized is held fixed at the geometry obtained from the previous iteration. Note that QM/MM interactions are also included at each iteration. The iterations are continued until the geometries of both systems no longer change.

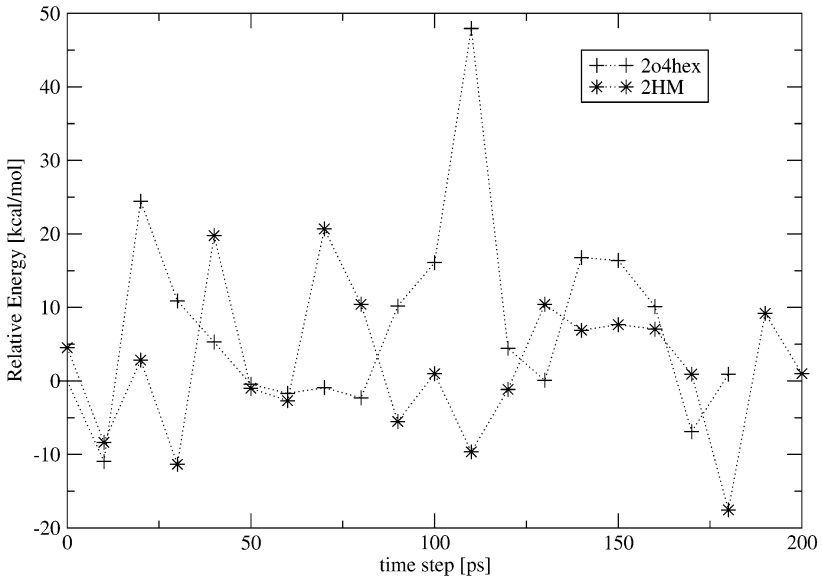

Figure 3. Relative energies for each snapshot in the MD simulation for 2o4hex and 2HM. All energies are relative to the initial energy of the 2o4hex intermediate.

The overall combined path optimization procedure is carried out in two steps. In the first step, the path is initially approximated by a series of structures obtained from a linear interpolation between the reactant and product structures using the core set of atoms. The environment set of one of these end points is employed for all the images on the path and the path is optimized with the NEB method for the core set with a loose convergence criteria. After each iteration on the core set, a restrained MM optimization as developed by Xie et al.[21] is carried out. Here, restraints are applied initially on the atoms of the environment set. These restraints are gradually reduced after each NEB/MM iteration until no restraints remain. The object of this restrained minimization is to ensure a smooth change in the environment set so that there are no sudden fluctuations which may cause one of the structures to move to a different minimum, which would result in the path being discontinuous.

In the second step, the converged path from the previous part is used as an initial guess for the parallel path optimizer method calculation to obtain the final optimized MEP. In this step the path is again iteratively optimized. However the restrained MM optimization is no longer performed, since the initial guess to the path is a much better approximation to the MEP.

2. Initial Structure Selection and Reaction Path Calculation. Preparation of the 4OT-substrate complexes as well as the details for the MD simulations have been explained in detail previously.[3,4] Briefly, the QM subsystem is composed of the substrate, Pro-1, and a water molecule in one of the active sites. These correspond to all molecules in a single stage in Figure 2 excluding the Arg residues. This results in a QM subsystem with 36 atoms including the pseudobond. The MM subsystem consists of 13161 atoms that include the rest of the enzyme and a 30 Å water sphere. This produces a total of 13197 atoms. Since our interest focuses on the selected active site, only atoms within 20 Å of the QM subsystem are allowed to move.

The initial structure for the determination of the potential energy paths for both 2HM and 2o4hex substrates was obtained from the calculated intermediate structures from our previous studies. For 2o4hex the intermediate was that obtained from[3] and for 2HM the intermediate was taken from.[4]

In principle, the absolute energy of the intermediate structures obtained from both reactants should be the same. In practice we found that the intermediate obtained from the 2o4hex path was 4.5 kcal/mol more stable than the one calculated from 2HM. This energy difference could be attributed to the influence that the enzyme environment plays on the energy in QM/MM calculations. For example, Zhang et al. have recently reported the effect of enzyme dynamics on QM/MM calculations on acetylcholinesterase (AChE).[22] They have determined that the enzyme environment may account for a change of ± 2 kcal/mol to the overall energy barrier on AChE.

On the basis of this fact we decided to study the effect of the enzyme environment on our calculations. To this end we generated 40 enzyme−substrate conformations by performing a 200 ps MD simulation on each intermediate structure (180 ps for 2o4hex). The structures for each substrate were obtained by choosing 20 equally spaced snapshots (including our initial structures) at 0, 10, 20, ..., 200 ps from our 200 ps MD simulation. Each structure was iteratively optimized using QM/MM methodology at the HF/3-21G level of theory. Figure 3 shows the calculated QM/MM energies of each structure for both MD simulations.

After this MD and minimization procedure we decided to employ the lowest calculated energy structure from both simulations as the initial MM environment. The reason is that, by definition, the lowest energy point will be the most probable structure from the ensemble and hence the most favored along the path. Also, our calculations provide only an upper bound to the true energies of the minimum points along the path, which justifies the use of the lowest calculated energy structure as a starting point for the determination of the reaction paths. This structure corresponds to the 180 ps snapshot of the 2HM MD simulation.

Three paths were approximated by linear interpolation using the intermediate structure with the lowest energy. The first path corresponds to the first step of the reaction with 2HM as the substrate, the second corresponds to the first step with 2o4hex, and the third corresponds to the second step of the reaction. In all cases the MM subsystem of the lowest intermediate was employed as the environment set for all the points on the paths. Note that for this reaction we only need to calculate the second step once because it is the same regardless of the initial substrate. Seven images were used for the representation of the first step of 4OT with 2o4hex as the substrate and for the representation

of the second step. In the case of the first step with 2HM as the substrate, 13 images were used to approximate the path (see Results section).

All paths were initially optimized in a series of NEB/MM optimization cycles employing the restrained MM optimization. After each NEB/MM cycle was completed, the convergence criteria for the core set was reduced. In the first cycle of the NEB optimization the path was considered converged when the gradient of the core set of atoms for all the points on the path was below 0.04 au. This criteria was reduced by 0.005 au in each cycle without going below 0.01 au for the last stages. In this case, since NEB is known to show fast convergence in the initial cycles, the maximum number of path optimization steps per cycle was set to 10.

In each NEB/MM cycle, a restrained minimization was performed on the environment set. In all cases, the environment set was required to converge to a gradient RMS of 0.1 kcal/mol Å^2 for all points. The positions of the active atoms in the environment set were restrained with a force constant of 500 kcal/mol in the first cycle, which was reduced in each subsequent cycle to 200, 100, 50, 25, and 10 kcal/mol. In the final cycle all restraints were removed to relax the environment.

Once the paths had converged with NEB, they were employed as an initial guess for the parallel path optimizer method. In this case we used the same convergence criteria as in our previous work.[13,14] All the points optimized to critical points were converged to the default criteria in Gaussian98. In the case of the uphill and downhill points the displacement criteria was reduced to half of the default.

The energies and gradients for the path optimizations were determined at the HF/3-21G level of theory for the NEB and parallel path optimizer method calculations. After the paths were optimized, a single point calculation on all images along the path was performed at the B3LYP/6-31G* and MP2/6-31G* levels. All paths have been optimized only at the HF level since the number of optimization iterations for a single elemental reaction step is relatively high, at least 300 steps,[14] which would be computationally expensive at the higher levels of theory.

For all calculations involving the MM subsystem (MM optimizations and MD simulations), because we do not simulate an infinite system, the conformational fluctuations of atoms near the boundary will not be realistic and thus were ignored. An active sphere with a radius of 20 Å centered around C-3 of the substrate in the QM subsystem was selected. All atoms outside this active sphere were constrained to their crystal structure positions. The twin range cutoff method[23] was used for nonbonded interactions with a long-range cutoff distance of 15 Å and a short-range cutoff of 8 Å. All MD simulations were carried out with a time step of 2.0 fs, maintaining a constant temperature of 300 K. In all cases the SHAKE[24] algorithm was employed to constrain all bond lengths of bonds involving hydrogen atoms.

To perform free energy perturbation (FEP) calculations on the optimized paths, points were added and optimized with a modified NEB method recently developed in our group.[25] In this method, after a path with a small number of images has been optimized, extra images are added between the optimized points. These images are optimized to the MEP with a modified NEB method, while the previously optimized points remain fixed. For the first step with 2o4hex, 19 points for the path, including the previously converged points, were used. In the case of the first step with 2HM as well as for the second step, 25 points were employed for the FEP determinations overall. Once the paths were converged with the modified NEB method, each point was allowed to equilibrate for 40 ps, followed by a period of 20 ps for the sampling of the free energy contributions.

The FEP calculations at the stationary points were further improved by determining the contributions from the fluctuations of the QM subsystem to the free energy difference.[11,12] These contributions were obtained by calculating the Hessian matrices of the stationary points for the core set of degrees of freedom and hence the vibrational frequencies with the quantum mechanical harmonic approximation. Once the vibrational frequencies were determined, the free energies for the stationary points and the free energy differences between them were obtained. All vibrational frequencies were calculated at the HF/3-21G level, with a scaling factor of 0.9409.[26]

B. Experimental Methods. *1. Materials.* Sodium dihydrogenphosphate was purchased from Sigma-Aldrich. The 2HM was kindly provided by Professor Christian P. Whitman (University of Texas at Austin), and wt-4OT was overexpressed in *Escherichia coli* cells and purified by reversed-phase high performance liquid chromatography (RP−HPLC).[27] The RP−HPLC purified material was folded by dissolving approximately 0.5−1.0 mg of material in 10−20 μL of 50 mM phosphate buffer (pH 8.5) containing 6.0 M guanidine hydrochloride (GuHCl). This solution of chemically denatured protein was diluted 50-fold into a 50 mM phosphate buffer (pH 8.5) and allowed to refold for at least 1 h at room temperature. Insoluble material was removed by centrifugation, and the folded 4OT hexamer was further purified by size exclusion chromatography (SEC).

The SEC was performed on a Dynamaz HPLC system using a superdex 75 HR 10/30 column (Pharmacia Biothech) and a flow rate of 1 mL/min. The mobile phase was 20 mM sodium phosphate buffer (pH 8.5) and the detector was set at 214 nm. The eluant from the 4OT hexamer peak in the SEC experiment was collected, and the pH adjusted to pH 7.0. the resulting 4OT sample was used directly for catalytic activity measurements.

2. Catalytic Activity Measurements. Catalytic activity measurements using 2HM as the enzyme substrate were performed as described in ref 8 with exception that absorbance measurements were made at 232 nm and not 236 nm. This was because the λ_{max} of the enzyme-reaction product, as determined on our Hewlett-Packard 8452A diode array UV−vis spectrophotometer, was 232 nm (4 nm lower than the same λ_{max} measured in ref 8).

Briefly, in the nonequilibrium experiments, a 1 μL aliquot of a 1−5 μM 4OT solution was added to 1 mL of 20 mM phosphate buffer (pH 7.0). Variable amounts (i.e., 0.5−20 μL) of a 20 mM 2HM stock solution in ethanol was immediately added to the assay solution. In the equilibrium experiments, the variable amounts of the 2HM stock solution were first added to the 1 mL of 20 mM phosphate buffer (pH 7.0), and then after a 4 min equilibration time, an aliquot of the 4OT stock solution (the same stock solution as the nonequilibrium experiments) was added to the assay solution. In both the equilibrium and nonequilibrium experiments, changes in absorbance at 232 nm were collected in 1 s intervals over a time period of 5 s.

The catalytic rate was determined in absorbance units per second by linear least-squares analysis of the raw absorbance data. The 20 mM phosphate buffer (pH 7.0) was used as blank in both experiments. In our enzyme assays, the final concentration of the enzyme was typically between 1 and 5 nM (as determined using the Waddell method[28]), and the final concentration of substrate was 10−400 μM. Initial velocity measurements were recorded in triplicate at least at five different concentrations of 2HM.

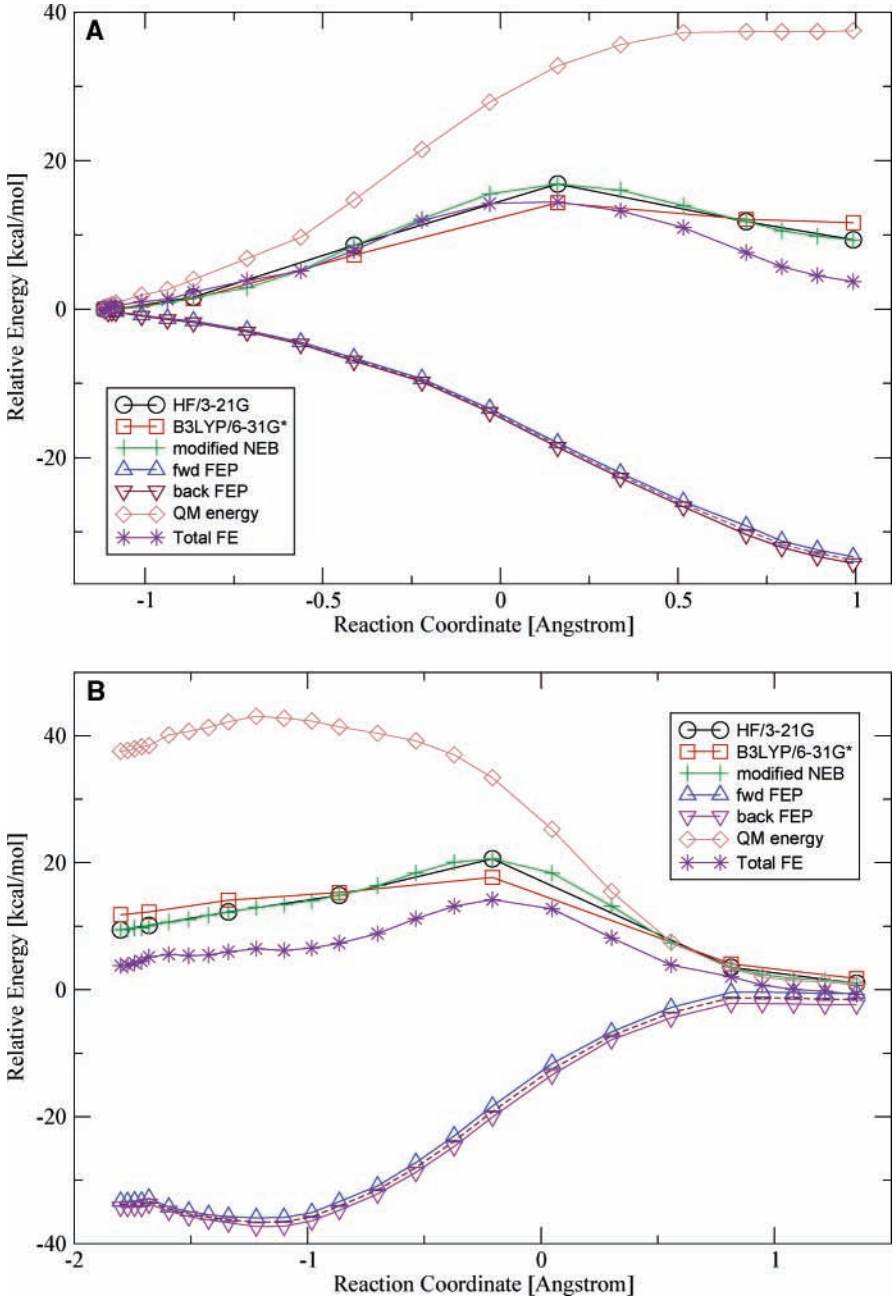

Figure 4. Relative potential and free energy paths for the first and second steps, A and B respectively, of the 4OT isomerization of 2o4hex.

III. Results and Discussion

A. QM/MM Potential Energies of Activation. The calculated reaction paths for both substrates are shown in Figures 4 and 5 for 2o4hex and 2HM, respectively. In all cases the calculated paths are reported relative to the corresponding reactant state. That is, the points along the paths for 2o4hex are reported relative to the reactant structure obtained from the calculation of the first step reaction for 2o4hex. For the 2HM paths all points are reported relative to the calculated 2HM reactant. For all paths, the reaction coordinates correspond to the distance difference between the breaking and forming bonds for each of the steps.

Tables 1 and 2 show the calculated potential energy barriers and the respective free energy barriers at three different levels of theory: HF/3-21G, B3LYP/6-31G*, and MP2/6-31G*. For the last two levels, single point calculations were performed at the higher levels of theory on the HF/3-21G optimized stationary points, to obtain the respective potential and free energy barriers. It is important to mention that since all structures were optimized at the HF/3-21G level, the determination of the frequencies and the contributions of the QM subsystem fluctuations to the free energy are only significant if they are done at at this level of theory. Thus, these were not calculated at the higher levels of theory (see Tables 1 and 2).

In the case of 2o4hex, the potential energy barrier for the first step is 16.85(14.32, 15.06) kcal/mol at the HF/3-21G(B3LYP/6-31G*, MP2/6-31G*) level and is centered around $R_1 = 0.16$ on the reaction coordinate as shown in Figure 4A. In the second step, the calculated potential energy barrier corresponds to 20.60(17.69, 20.47) kcal/mol (see Figure 4B) and is centered around $R_2 = -0.2$. These results suggest that the second step is the rate-limiting step, in agreement with experimental findings.[8,29] The associated free energy barrier corresponds to 13.69(11.19, 11.36) and 13.67(10.76, 13.60) kcal/mol for the

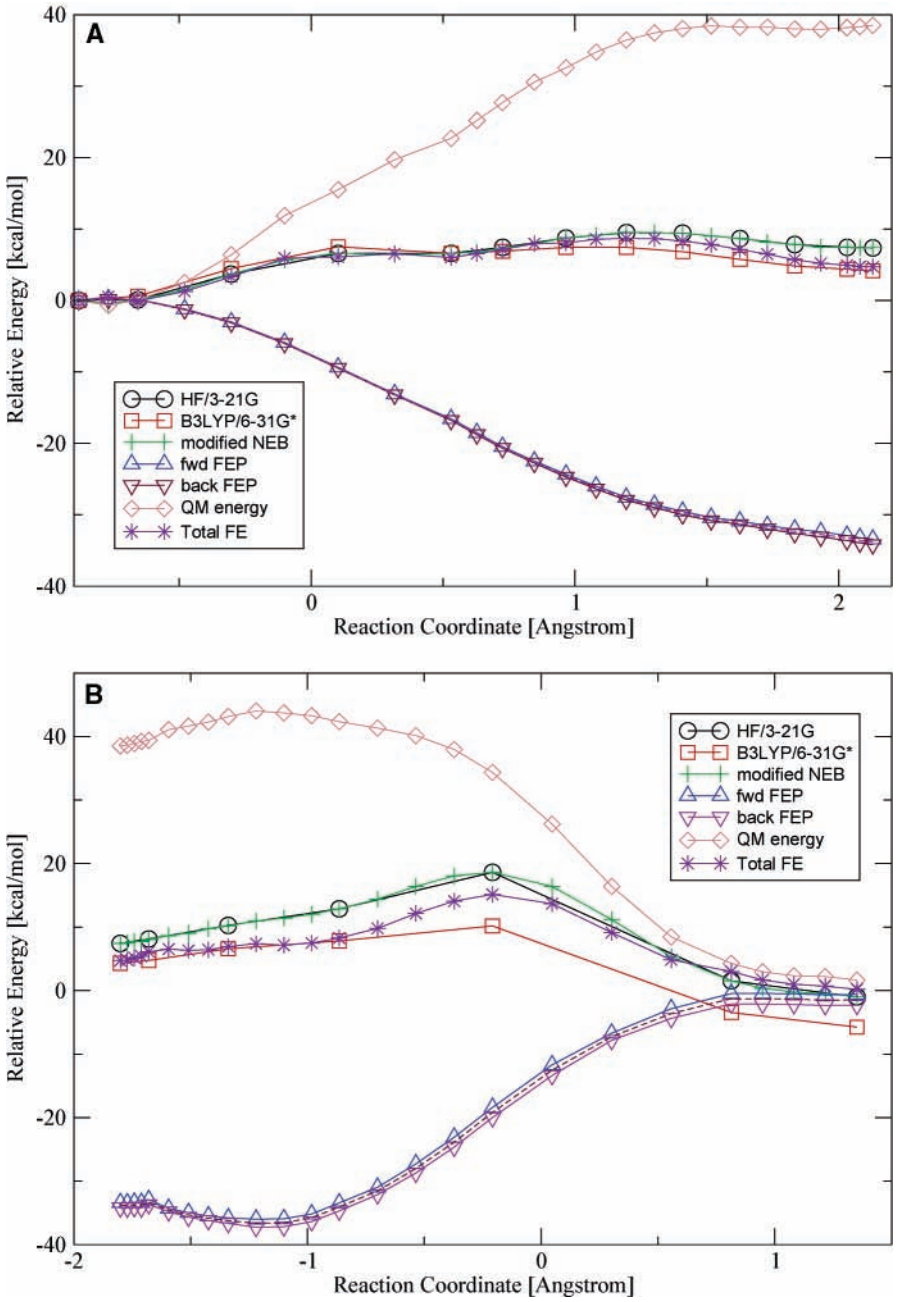

Figure 5. Relative potential and free energy paths for the first and second steps, A and B respectively, of the 4OT isomerization of 2HM.

first and second steps, respectively. In this case the calculated energy barrier difference is too small to determine which step is rate determining, except for the MP2 result (see Table 1).

For 2HM, we found that the first step presents two barriers of 6.59(7.50, 7.60) and 9.42(7.43,8.19) kcal/mol at the HF/3-21G(B3LYP/6-31G*, MP2/6-31G*) level (see Figure 5A). The first barrier is centered around $R_1 = 0.1$ along the reaction coordinate and corresponds to the proton transfer from the substrate to Pro-1.[4] However, immediately after this transfer takes place, a stable intermediate (I1, see Table 2) is formed centered around $R_1 = 0.5$; this intermediate is characterized by a hydrogen bond (H-bond) between the three atoms involved in the reaction. The second barrier is centered around $R_1 = 1.2$ and corresponds to the breaking of this H-bond and the subsequent rearrangement of the substrate in the active site. In this case, 13 images were required to approximate this path for the combined path optimization procedure in order to correctly map both energy barriers associated with this step.

The calculated potential energy barrier for the second step with 2HM is 18.61(10.18, 12.55) kcal/mol, and is centered around $R_2 = -0.2$ as shown in Figure 5B. The calculated results for 2HM also show that the second step is the rate-limiting step, in agreement with 2o4hex and experimental determinations. Note that for both substrates, the second step is centered around the same place in the reaction path. This is because the second step for both substrates is the same since we start the reaction from the same intermediate as noted previously. However, the energy barriers for the second steps are calculated relative to the reactants. Since the reactants for the 2o4hex and 2HM reactions differ, they have different energies. Hence we observe a difference in the calculated energy barriers for the second steps between the two substrates.

An interesting feature arises when the associated free energy is calculated for the 2HM paths, in that the first step presents a single barrier of 12.82(7.60,8.36) kcal/mol centered on the first intermediate for HF and on the second TS for B3LYP and MP2

TABLE 1: Calculated Potential and Free Energy Differences for the Isomerization of 2o4hex by 4OT (in kcal/mol)[a]

structure	ΔE	ΔE_{QM}	$\Delta F_{QM/MM}$	$\Delta F^{fluct}_{QM/MM}$	ΔF
TS1[b]	16.85	32.75	−18.30	−0.76	13.69
I[b]	9.34	37.50	−33.79	2.48	6.19
TS2[b]	20.60	33.38	−19.19	−0.52	13.67
P[b]	0.99	0.69	−1.46	0.47	−0.30
TS1[c]	14.32	30.25	−18.30	−0.76	11.19
I[c]	11.64	39.81	−33.79	2.48	8.50
TS2[c]	17.69	30.47	−19.19	−0.52	10.76
P[c]	1.76	1.47	−1.46	0.47	0.48
TS1[d]	15.06	30.42	−18.30	−0.76	11.36
I[d]	13.82	42.06	−33.79	2.48	10.75
TS2[d]	20.47	33.31	−19.19	−0.52	13.60
P[d]	2.42	2.23	−1.46	0.47	1.24

[a] All energies are relative to the reactant. ΔE is the total potential energy difference, and ΔE_{QM} refers to the QM energy difference between two QM subsystems. $\Delta F_{QM/MM}$ is the free energy change in the QM/MM interaction, $\Delta F^{fluct}_{QM/MM}$ refers to the contribution of the QM subsystem fluctuations to the free energy, and $\Delta F = \Delta E_{QM} + \Delta F_{QM/MM} + \Delta F^{fluct}_{QM/MM}$. [b] Values determined at the HF/3-21G level for the QM energy. [c] Values determined at the B3LYP/6-31G* level. [d] Values determined at the MP2/6-31G* level.

TABLE 2: Calculated Potential and Free Energy Differences for the Isomerization of 2HM by 4OT (in kcal/mol)[a]

structure	ΔE	ΔE_{QM}	$\Delta F_{QM/MM}$	$\Delta F^{fluct}_{QM/MM}$	ΔF
TS1[b]	6.59	15.50	−9.41	−1.40	4.69
I1[b]	6.57	28.68	−16.67	0.81	12.82
TS2[b]	9.42	36.44	−27.75	0.92	9.61
I2[b]	7.45	38.50	−33.79	−0.01	4.70
TS3[b]	18.61	34.33	−19.19	−2.97	12.17
P[b]	−0.99	1.65	−1.46	−1.99	−1.80
TS1[c]	7.50	16.43	−9.41	−1.40	5.62
I1[c]	6.59	23.31	−16.67	0.81	7.45
TS2[c]	7.43	34.43	−27.75	0.92	7.60
I2[c]	4.13	35.31	−33.79	−0.01	1.51
TS3[c]	10.18	25.91	−19.19	−2.97	3.75
P[c]	−5.74	−3.08	−1.46	−1.99	−6.53
TS1[d]	7.60	16.56	−9.41	−1.40	5.75
I1[d]	7.46	23.62	−16.67	0.81	7.76
TS2[d]	8.19	35.19	−27.75	0.92	8.36
I2[d]	5.90	37.06	−33.79	−0.01	3.26
TS3[d]	12.55	28.29	−19.19	−2.97	6.13
P[d]	−5.49	−2.77	−1.46	−1.99	−6.22

[a] All energies are relative to the reactant. ΔE is the total potential energy difference, and ΔE_{QM} refers to the QM energy difference between two QM subsystems. $\Delta F_{QM/MM}$ is the free energy change in the QM/MM interaction, $\Delta F^{fluct}_{QM/MM}$ refers to the contribution of the QM subsystem fluctuations to the free energy, and $\Delta F = \Delta E_{QM} + \Delta F_{QM/MM} + \Delta F^{fluct}_{QM/MM}$. [b] Values determined at the HF/3-21G level for the QM energy. [c] Values determined at the B3LYP/6-31G* level. [d] Values determined at the MP2/6-31G* level.

(see Table 2). In this case the contributions of the MM environment produce the stabilization of the first transition state for this step and result in the appearance of only one barrier in the free energy regime. The associated free energy for the second step is 12.17(3.75,6.13) kcal/mol. The free energy barrier determined with QM energy differences at the HF level is too close to the energy barrier of the first step to determine which step is rate determining in the free energy landscape, as was the case for 2o4hex. For the free energy barriers determined with the higher levels of theory, we observe a switch in the rate-limiting step for this substrate to the first step of the reaction.

As can be seen from Tables 3 and 4, the calculated structures for the reactant, product, and intermediates correspond to true minima along the PES since there are no imaginary frequencies.

TABLE 3: Lowest Vibrational Frequencies for Stationary Points on the Paths for 4OT with 2o4hex, Frequencies in cm^{-1}

reactant	TS1	I1	TS2	product
60.65	−1417.71	62.40	−1392.72	68.34

TABLE 4: Lowest Vibrational Frequencies for Stationary Points on the Paths for 4OT with 2HM, Frequencies in cm^{-1}

reactant	TS1	I1	TS2	I2	TS3	product
66.12	−949.20	63.64	−100.98	62.40	−1392.72	68.34

In the case of the transition states, a single negative frequency was observed, which shows that these structures are true first-order saddle points.

The difference between the potential energy barriers for the rate-limiting steps for 2o4hex and 2HM yield $\Delta\Delta E$s of 1.99, 7.51, and 7.92 kcal/mol at the HF/3-21G, B3LYP/6-31G*, and MP2/6-31G* levels, respectively. In the case of the barrier differences for the associated free energies at the three levels of theory, the calculated $\Delta\Delta G$ including the fluctuations of the QM subsystem are 0.87, 3.59, and 5.24 kcal/mol. These results show that all three methods qualitatively agree on 2HM as the substrate which is turned-over faster by 4OT than 2o4hex. These results also agree with our experimental free energy difference ($\Delta\Delta G$) of 0.85 kcal/mol (see Subsection IIIB). It is important to note, however, that these energy differences are very small at the HF/3-21G level at which all structures were optimized, which indicates that both substrates should be considered.

A large energy difference is observed between the $\Delta\Delta E$s and $\Delta\Delta G$s calculated with B3LYP and MP2 compared with the HF results. In both cases these differences come from the QM contributions to the energy. These differences may be due in part to the fact that the structures were optimized only at the HF/3-21G level; only a single point calculation at the higher level was performed on these geometries.

Note that the calculated rate-limiting free energy barriers for 2HM and 2o4hex at the HF/3-21G level, 12.82 and 13.69 kcal/mol, respectively, are both in better agreement with the experimental activation barrier of 13 kcal/mol[30,31] than our previously calculated free energy barrier for 2o4hex of 16.45 kcal/mol.[3] This lowering in the free energy barrier is explained by the use of a much more relaxed initial enzyme environment for the path determinations, and by the use of a better MEP solver in the present work. The good agreement of the calculated energy barriers with the experimental one shows that the determination of reaction mechanisms at a relatively low level of theory (HF/3-21G) produces good theoretical results. This is most likely due to error cancellation.

Our calculations for the reaction paths for both substrates starting from the same intermediate are in agreement with our previous calculations for the reaction mechanism of 4OT.[3,4] In the first step, we observe a water molecule that approaches the carbonyl (hydroxyl) oxygen in the intermediate, where the negative charge is formed. This water molecule, labeled H_2O-2 as in our previous studies, is observed to come within a distance of ≈3 Å from the oxygen where the negative charge is formed in the intermediate structure (see Figure 5 in ref 3) regardless of the substrate. In the second step, this water molecule gets further away from the site of the negative charge as the product is formed.

B. Experimental Results. A nonequilibrium experiment where 2HM is the substrate and an equilibrium experiment where both 2HM and 2o4hex are substrates are performed to determine which substrate is better for 4OT catalysis. In accordance with Michaelis−Menten kinetics, the kinetic pa-

TABLE 5: Kinetic Parameters Derived from Nonequilibrium and Equilibrium Experiments

substrate	K_M (μM)	k_{cat} (s^{-1})	k_{cat}/K_M ($M^{-1}\,s^{-1}$)	$\Delta G^{\ddagger}$
2HM	121 ± 16	2092 ± 200	$(1.74 \pm 0.11) \times 10^7$	12.92 ± 0.06
2HM and 2o4hex	90 ± 20	1142 ± 230	$(1.37 \pm 0.23) \times 10^7$	13.28 ± 0.12
2o4hex	59 ± 22	498 ± 61	$(0.82 \pm 0.32) \times 10^7$	13.77 ± 0.08

rameters K_M, k_{cat}, and k_{cat}/K_M for 2HM and for the mixture of 2HM and 2o4hex were determined from the data collected in both the nonequilibrium and the equilibrium experiments (Table 5). Note that the spectrophotometric enzyme assay used in this work involved monitoring the rate of product formation. In the nonequilibrium experiment 2HM was assumed to be the only substrate. However, in the equilibrium experiment both 2HM and 2o4hex were assumed to be present as substrates. The kinetic parameters for 2o4hex were determined using the velocity equation derived from a model in which two substrates (2HM and 2o4hex) compete for the same active site of enzyme (Table 5).[8] The activation energy barriers ($\Delta G^{\ddagger}$) obtained using the transition state theory are also listed in Table 5. The calculated free energy barrier difference $\Delta\Delta G$ ($\Delta G_{2o4hex} - \Delta G_{2HM}$) is 0.85 ± 0.1 kcal/mol. This is in good agreement with the theoretical calculations reported above.

Our experimental results indicate that 2HM is turned over by 4OT faster than 2o4hex is turned over by 4OT. It is noteworthy that this is different from the conclusion reached in ref 8. In ref 8, 2o4hex was found to be a slightly better substrate than 2HM. The enzyme assay conditions and experimental protocols used in the present work were identical to those used in ref 8 with only two minor exceptions. One exception was that the enzyme concentration was calculated based on the active enzyme complex being a hexamer (not as a tetramer as it was thought to be at the time ref 8 was published). These different methods for enzyme quantitation are expected to impact the relative magnitudes of the k_{cat} parameters measured in the two studies; but they are not expected to impact the relative measurements made within each study. The second exception was that absorbance measurements at 232 nm were performed in the enzyme assay instead of absorbance measurements at 236 nm. This change was made to ensure that the absorbance measurements in the current work were being conducted at the λ_{max} of the product, which was 232 nm as measured using the spectrophotometer in this work and 236 nm as measured using the spectrophotometer in ref 8.

It is also noteworthy that the techniques we have employed for enzyme purification and characterization are different from those employed in ref 8. One notable difference is that our purification and characterization of the 4OT material used in the current work, included a RP−HPLC purification and an electrospray ionization mass spectrometry analysis to confirm the enzyme's purity. Unfortunately, the high sensitivity of electrospray ionization was not exploited in ref 8 as the field of protein mass spectrometry was only in very early stages of development at the time the work in ref 8 was performed. The discrepancy between the experimental results reported here and those reported in ref 8 could be explained by the presence of protein impurities with 2o4hex isomerization activity in the enzyme preparation used in ref 8.

IV. Conclusions

We have studied which substrate, 2o4hex or 2HM, is turned over faster by 4OT by means of a combined QM/MM method and experimental kinetic determinations. Reaction paths for both steps of the reaction, with both substrates, have been theoretically calculated to obtain the energy barriers for the reactions. Catalytic determinations were done experimentally for both substrates, and energy barriers were obtained with the transition state theory to compare with theoretical results.

Theoretically, the rate-limiting energy barrier ($\Delta\Delta E$) difference between 2o4hex and 2HM at three different levels of theory, 1.99, 7.51, and 7.92 kcal/mol, as well as the calculated free energy barrier difference of 0.87, 3.59, and 5.24 kcal/mol, point to 2HM as the substrate which is turned over faster by 4OT. Our experimental kinetic studies yield a $\Delta\Delta G = 0.85$ kcal/mol, in qualitative agreement with our theoretical determinations. These results suggest that both substrates need to be taken into account.

The calculated reaction paths for both substrates were determined from the same initial intermediate. In both cases, the calculated paths agree with the previously determined paths.[3,4] Our calculations confirm that no residue or water molecule act as a general acid in the reaction. The negative charge formed in the intermediate state is stabilized by Arg-39″ and an ordered water in the active site.

Acknowledgment. Support from the National Institute of Health is gratefully acknowledged. G.A.C. thanks the CONACyT for financial support.

References and Notes

(1) Chen, L. H.; Kenyon, G. L.; Curtin, F.; Harayama, S.; Bembenek, M. E.; Hajipour, G.; Whitman, C. P. *J. Biol. Chem.* **1992**, *267*, 17716.

(2) Harayama, S.; Rekik, M.; Ngai, K. L.; Ornston, L. N. *J. Bacteriol.* **1989**, *171*, 6251.

(3) Cisneros, G. A.; Liu, H.; Zhang, Y.; Yang, W. *J. Am. Chem. Soc.* **2003**, *134*, 10348−10393.

(4) Cisneros, G. A.; Wang, M.; Silinski, P.; Fitzgerald, M. C.; Yang, W. *Biochemistry* **2004**, *43*, 6885−6892.

(5) Metanis, N.; Brik, A.; Dawson, P. E.; Keinan, E. *J. Am. Chem. Soc.* **2004**, *126*, 12726−12727.

(6) Czerwinski, R. M.; Harris, T. K.; Massiah, M. A.; Mildvan, A. S.; Whitman, C. P. *Biochemistry* **2001**, *40*, 1984.

(7) Harris, T. K.; Turner, G. J. *IUBMB Life* **2002**, *53*, 85−98.

(8) Whitman, C. P.; Aird, B.; Gillespie, W.; Stolowich, N. *J. Am. Chem. Soc.* **1991**, *113*, 3154.

(9) Warshel.; Levitt, *J. Mol. Biol.* **1977**, *103*, 227.

(10) Zhang, Y.; Lee, T.; Yang, W. *J. Chem. Phys.* **1999**, *110*, 46.

(11) Zhang, Y.; Liu, H.; Yang, W. *J. Chem. Phys.* **2000**, *112*, 3483.

(12) Zhang, Y.; Liu, H.; Yang, W. Ab Initio QM/MM and Free Energy Calculations of Enzyme Reactions. In *Computational Methods for Macromolecules-Challenges and Applications*; Springer-Verlag: Heidelberg, Germany, 2002.

(13) Liu, H.; Lu, Z.; Cisneros, G. A.; Yang, W. *J. Chem. Phys.* **2004**, *121*, 607−706.

(14) Cisneros, G. A.; Liu, H.; Lu, Z.; Yang, W. *J. Chem. Phys.* **2005**, *122*, 114502.

(15) Frisch, M. J.; et al. *Gaussian 98, Revision A.8*; Gaussian, Inc.: Pittsburgh, PA, 1998.

(16) Ponder, J. *TINKER, Software Tools for Molecular Design, Version 3.6*: (the most updated version for the TINKER program can be obtained from Ponder's website at http://dasher.wustl.edu/tinker); Washington University: St. Louis, MO, 1998.

(17) Cornell, W. D.; Cieplak, P.; Bayly, C. I.; Gould, I. R.; Merz, K. M.; Ferguson, D. M.; Spellmeyer, D. C.; Fox, T.; Caldwell, J. W.; Kollman, P. A. *J. Am. Chem. Soc.* **1995**, *117*, 5179.

(18) Jorgensen, W.; Chandrasekhar, J.; Madura, J.; Impey, R.; Klein, M. *J. Chem. Phys.* **1983**, *79*, 926.

(19) Jónsson, H.; Mills, G.; Jacobsen, K. Nudged Elastic Band Method. In *Classical and quantum dynamics in condensed phase simulations*; World Scientific: Singapore, 1998.

(20) Henkelman, G.; Jónsson, H. *J. Chem. Phys.* **2000**, *113*, 9978−9985.

(21) Xie, L.; Liu, H.; Yang, W. *J. Chem. Phys.* **2004**, *120*, 8039−8052.
(22) Zhang, Y.; Kua, J.; McCammon, J. *J. Phys. Chem. B* **2003**, *107*, 4459−4463.
(23) van Gunsteren, W.; Berendsen, H.; Colonna, F.; Perahia, D.; Hollenberg, J.; Lellouch, D. *J. Comput. Chem.* **1984**, *5*, 272.
(24) Ryckaert, J.; Ciccotti, G.; Berendsen, H. *J. Comput. Phys.* **1977**, *23*, 327.
(25) Cisneros, G. A.; Yang, W. *J. Chem. Phys.*, to be submitted.
(26) Foresman, J.; Frisch, A. *Exploring Chemistry with Electronic Structure Methods*; Gaussian Inc.: Pittsburgh, PA, 1996.
(27) Silinski, P.; Allingham, M. J.; Fitzgerald, M. C. *Biochemistry* **2001**, *40*, 4493.
(28) Waddel, W. J. *J. Cab. Clin. Med.* **1956**, *48*, 311−314.
(29) Stivers, J. T.; Abeygunawardana, C.; Mildvan, A. S.; Hajipour, G.; Whitman, C. P. *Biochemistry* **1996**, *35*, 814.
(30) Czerwinski, R. M.; Johnson, W. H. Jr.; Whitman, C. P.; Harris, T. K.; Abeygunawardana, C.; Mildvan, A. S. *Biochemistry* **1997**, *36*, 14551.
(31) Harris, T. K.; Czerwinski, R. M.; Johnson, W. H., Jr.; Legler, P. M.; Abeygunawardana, C.; Massiah, M. A.; Stivers, J. T.; Whitman, C. P.; Mildvan, A. S. *Biochemistry* **1999**, *38*, 12343.